ACS SENSORS

pubs.acs.org/acssensors Article

Multiplexed Salivary miRNA Quantification for Predicting Severe COVID-19 Symptoms in Children Using Ligation-RPA Amplification Assay

Md. Ahasan Ahamed, Zhikun Zhang, Aneesh Kshirsagar, Anthony J. Politza, Usha Sethuraman, Srinivasan Suresh, Steven Hicks, Feng Guo, and Weihua Guan*

Cite This: *ACS Sens.* 2025, 10, 5150−5159 Read Online

ACCESS | Metrics & More | Article Recommendations | Supporting Information

ABSTRACT: While most children with COVID-19 experience mild symptoms or remain asymptomatic, some may develop severe complications. Early identification of children at risk for severe outcomes is essential to ensuring timely and effective intervention. Recent studies have identified alterations in salivary microRNA (miRNA) expression levels as promising biomarkers for predicting severe complications in children. However, there remains a need for a rapid, noninvasive, and quantitative method to detect miRNA expression level changes, as their upregulation or downregulation serves as a hallmark of various diseases, providing an alternative to sequencing-based methods. Here, we developed a highly specific and sensitive ligation-coupled recombinase polymerase amplification (RPA) assay for quantitatively detecting multiplex severe and nonsevere miRNAs on a portable platform. The assay begins with an miRNA-templated annealing and ligation reaction of miR-1273, miR-296, and miR-29, followed by an RPA reaction. We quantified 100 pM to 1 fM, resolving 1 fM, with 100% specificity. Next, we validated portable extraction against benchtop extraction, achieving $R^2 > 0.85$ and $r > 0.92$ in clinical samples. Finally, testing 154 clinical samples revealed severe miRNA downregulation compared to nonsevere cases. The assay achieved high diagnostic accuracy with an area under the curve (AUC) of 0.98. This platform would empower clinicians to make informed decisions, optimize resource allocation, and improve outcomes, particularly in point-of-care (POC) settings.

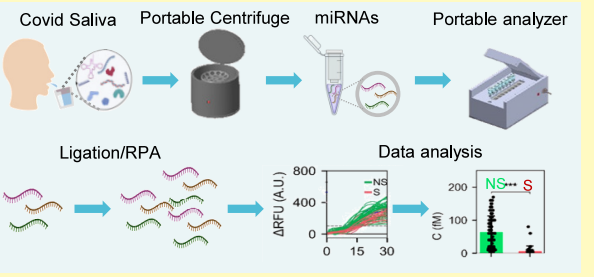

KEYWORDS: *SARS-CoV-2, salivary miRNAs, ligation-RPA reaction, recombinase polymerase amplification, portable analyzer, portable centrifuge, severe COVID-19, point-of-care*

The true prevalence of asymptomatic Severe acute respiratory syndrome coronavirus 2 (SARS-CoV-2) infections in children is likely underestimated, as many remain undiagnosed due to mild or absent symptoms. Most pediatric COVID-19 cases are mild, yet a notable minority develop serious outcomes such as multisystem inflammatory syndrome in children (MIS-C), severe pneumonia or Acute Respiratory Distress Syndrome (ARDS), cardiac or clotting disorders, worsened chronic illnesses, and occasional neurologic events.[1−3] By mid-2023, the pandemic had caused roughly 767.97 million cases and nearly 7 million deaths; UNICEF notes more than 17,400 COVID-19 deaths among people under 20 years, about half in children under 10 years.[4,5] Severe SARS-CoV-2, while less common in children, can lead to serious complications.[6] Early identification of high-risk cases is crucial to ensure timely treatment, proper patient management, and effective use of healthcare resources.[7] Due to its noninvasive and easily accessible nature, saliva is a promising sample for POC.[8−10] Saliva contains DNA and RNA biomolecules, including miRNAs, which serve as useful biomarkers for detecting various infectious diseases.[1,11,12] MiRNAs are short noncoding RNAs that regulate gene expression and influence immune responses.[13,14] Salivary miRNA levels reflect inflammation, and the relative abundance of multiple salivary miRNAs has been investigated as biomarkers for SARS-CoV-2.[1,15−17] Consequently, developing multiplexed and quantitative miRNA detection in saliva is critical for the early detection of a severe SARS-CoV-2 infection in children.

Numerous methods have been developed for miRNA detection,[18,19] including Northern blot,[20] microarray,[21] and reverse transcription-polymerase chain reaction (RT-PCR).[22] Northern blotting offers high specificity but is time-consuming and requires large sample volumes. Microarrays allow high-throughput profiling but are costly and complex.[23−25] RT-PCR

Received: April 16, 2025
Revised: June 25, 2025
Accepted: June 27, 2025
Published: July 4, 2025

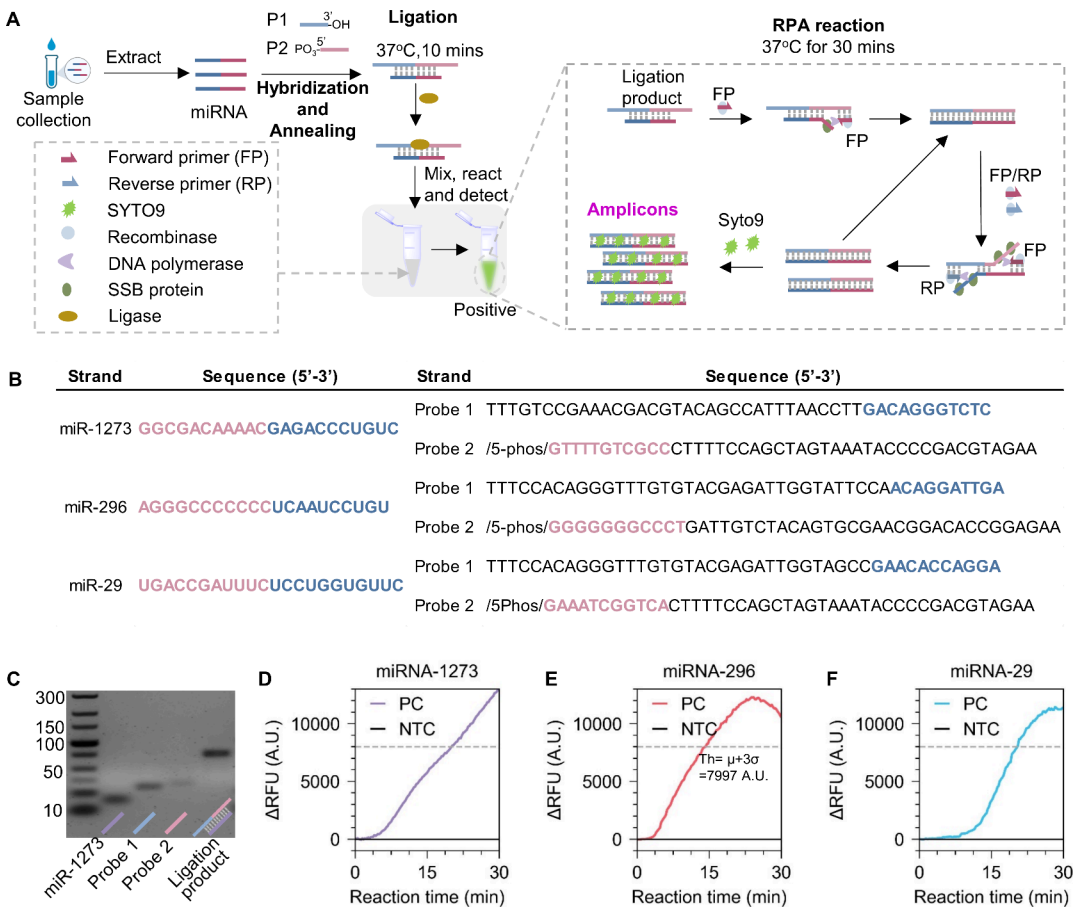

Figure 1. Schematic illustration of ligation-RPA assay for SARS-CoV-2 miR-1273, miR-296, and miR-29 and validation using the benchtop instrument. (A) Operation workflow of the ligation-RPA assay. The sample was extracted from saliva, followed by hybridization at 85 °C for 2 min, annealing, ligation reaction at 37 °C for 10 min, and RPA amplification at 37 °C for 30 min. The forward primer (FP) and reverse primer (RP) bind with ligation products, and SYTO 9 inserts into the base pair of dsDNA. (B) Probes of miR-1273, miR-296, and miR-29 are used in ligation-RPA assay. (C) Validation of miR-1273 Ligation product using gel image. Ligation products showed an intense mark near 75 bp. (D–F) Delta Relative fluorescence signal (ΔRFU) for positive samples for miR-1273, miR-296, and miR-29, respectively. The threshold (Th) was set using $\mu + 3\sigma$= 7997 A.U., where μ and σ indicate the mean and standard deviation, respectively.

is highly sensitive and accurate but depends on thermal cycling, limiting its suitability for POCT.[10,26] To overcome these limitations, isothermal amplification methods such as nucleic acid sequence-based amplification (NASBA),[27] strand displacement amplification (SDA),[28] rolling circle amplification (RCA),[29] loop-mediated isothermal amplification (LAMP),[30] and recombinase polymerase amplification (RPA)[31−34] have been explored. Among them, RPA is widely favored for its simplicity, sensitivity, rapid amplification, and operation at 37−42 °C.[35] However, RPA is challenged by short length of miRNA, as it typically requires amplicons longer than 80 bp.[36] This limitation can be addressed using PBCV-1 DNA ligase with RPA,[37,38] enabling longer products and achieving PCR-like sensitivity for rapid miRNA detection in point-of-care Testing (POCT) applications. Recent studies identified miRNA (miR)-1273c and miR-296 as two of the most down-regulated miRNAs in severe cases, while the miR-29 family is a well-established regulator of innate immunity.[1,16,39] Consequently, we selected miR-1273c, miR-296-5p, and miR-29 as targets to demonstrate the clinical utility of our ligation-RPA assay. A key challenge in previous work is the lack of an end-to-end portable system capable of measuring pediatric SARS-CoV-2 miRNAs in saliva at femtomolar (fM) resolving capacity.[40,41] Therefore, there is an unmet need for a rapid, noninvasive, and quantitative method to detect miRNA expression level changes in fM level and enable early risk for severe SARS-CoV-2 infection in children.

In this work, we developed a ligation-RPA-based isothermal nucleic acid amplification system for detecting miRNAs associated with severe SARS-CoV-2 infection using a portable analyzer. Our system successfully multiplexed and detected three miRNAs- miR-1273, miR-296, and miR-29 for SARS-CoV-2 infection, quantifying their concentrations to establish the clinical relevance fM concentration. We validated the specificity of the system with both individual and mixed samples, demonstrating that our portable extraction method exhibited performance comparable to that of benchtop systems. Using this portable platform, we were able to differentiate between severe and nonsevere infections from raw salivary samples, showing the downregulation of specific miRNAs in severe cases. Our platform offers significant potential for early disease diagnosis and practical application in POCT.

RESULTS AND DISCUSSION

Design and Validation of the Ligation/RPA Assay. We designed and developed the ligation-RPA assay to enable the rapid, sensitive, and specific detection of salivary SARS-CoV-2

https://doi.org/10.1021/acssensors.5c01275
ACS Sens. 2025, 10, 5150−5159

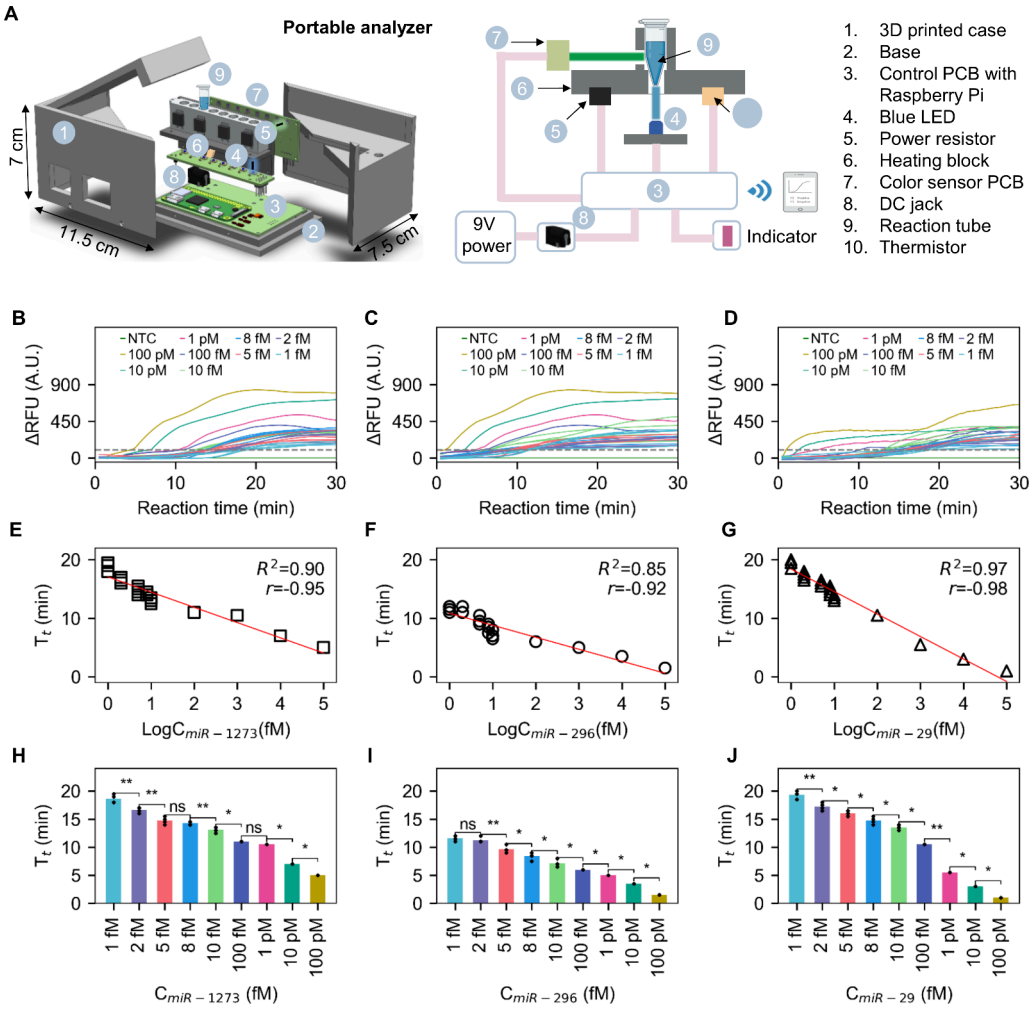

Figure 2. Quantitative performance and sensitivity of the assay. (A) Exploded view and schematic of the portable analyzer. (B–D) Quantitative analysis showing the ΔRFU of miR-1273, miR-296, and miR-29 at target concentrations of 100 pM, 10 pM, 1 pM, 100 fM, 10 fM, 8 fM, 5 fM, 2 fM, and 1 fM, respectively. The gray dashed line represents the threshold ($\mu + 3\sigma$ = 100.43 A.U.), where μ and σ denote the mean and standard deviation. (E–G) The assay demonstrates linearity by plotting time-to-positive (T_t) against the logarithm of the concentration for each miRNA target exceeding the threshold. (H–J) Assay resolution shown using *t*-test results to evaluate resolving capabilities. 'ns' indicates 'no significance', while * and ** denote 'statistically significant differences'.

miRNAs in children. The assay starts with hybridization between miRNA and probes 1 and 2 (P1 and P2), enhanced by rapid denaturing at 85 °C for 2 min, followed by 2 min annealing on an ice bath, as shown in Figure 1A. Following hybridization, P1 and P2 formed a phosphodiester bond between the 3′-hydroxyl(−OH) group of P1 and the 5′-phosphate (PO_4^{3-}) of P2, effectively stabilizing the hybridized structure and creating 5′-phosphorylated single-strand DNA (ssDNA).[40] Next, PBCV-1 DNA ligase catalyzed and bridged of the 5′ to 3′ terminals of the complementary sequence of probes P1 and P2 with 3′ to 5′ terminals of the target miRNA oligonucleotides, synthesizing a partially double-stranded structure.[37] The ligation reaction works at 37 °C for 10 min; P1 and P2 were designed to partially hybridize with the target miRNA and linked to a long ssDNA (ligation products). The ligation products specifically linked with forward primer (FP) and reverse primer (RP) sites in the RPA reaction were effectively and specifically amplified at 37 °C for 30 min. Intercalating dyes SYTO 9 bind to RPA amplicons by inserting themselves between the base pairs of the double-stranded DNA (dsDNA) formed during amplification.[42] The planar structure of the dye allows it to insert into the hydrophobic space between stacked DNA base pairs, stabilized by hydrophobic and electrostatic interactions with the negatively charged phosphate backbone. Once intercalated, the dye fluoresces, enabling the detection and quantification of the amplified product. In Figure 1B, the target sequences of miR-1273, miR-296, and miR-29, and the probe sequences P1 and P2 are shown.

To validate the ligation assay, we verified the ligation reaction by testing the miR-1273, P1, P2, and ligation products using agarose gel electrophoresis (Figure 1C). The results showed that the ligation product band was intense and brighter than the miR-1273, P1, and P2 bands because the larger, high-molecular-weight ligation products moved more slowly than the tiny fragments of ssDNA. These results demonstrated that ligation products, including P1 and P2 sequences, were successfully synthesized in the presence of miR-1273. To revalidate the ligation-coupled RPA reaction, we tested 100 pM target concentrations of miR-1273, miR-296, and miR-29. We used an interacting fluorescent dye (SYTO 9) in real-time quantitative measurement of the RPA assay to determine the

https://doi.org/10.1021/acssensors.5c01275
ACS Sens. 2025, 10, 5150−5159

change in the Relative Fluorescence Units (ΔRFU) signal of miR-1273, miR-296, and miR-29. Figure 1D shows a noticeable signal time difference between positive controls (PC) and negative controls (NTC) at the threshold lines (μ + 3σ= 7997 AU). Ideally, the NTC should not pick up any signal. However, the NTC shows signal lagging from the PC due to nonspecific amplification, as shown in Figure S1A−C. NTC also showed an increase in fluorescent signal with the reaction time in the ligation-RPA platform. It indicated that there was a nonspecific amplification due to the nonspecific binding of probes and primers. Our assay had two probes (P1 and P2) and primers (FP and RP). P2 can directly hybridize with FP to form double-strand DNA (dsDNA) and nonspecific products (Figure S2A). Furthermore, P1 and P2 form self/hetero dimers and can be amplified to nonspecific products due to cross-dimerization in isothermal amplification;[43−45] see Figure S2B.

To validate our investigation of nonspecific bindings from negative signals by self- or heterodimer amplification, we sequentially added P1, P2, RP, FP, and their various mixtures into the RPA amplification system. Next, a commercial enzyme digestion kit was used to break down proteins, allowing for selective detection of amplicons via gel electrophoresis (Figure S2C). It showed that RPA invariably forms large amounts of side products in practice, which come from hybridizing P1 and P2 as well as P2 and FP and probes dimers, called primer-dimers.[45,46] High concentrations of probes encourage off-target interactions because the amplification of probe dimers is more efficient than the amplification of the desired amplicons, and probe−probe interactions eventually eliminate target amplification.[44,47] We therefore carried out a systematic concentration screen for miR-29 (Figure S2D−H). Varying each probe from 10 pM to 1 μM of P2 revealed that 100 nM P1 and 100 nM P2 maximized the time gap ($\Delta t \approx$ 14.5 min) between the PC and NTC, indicating the best discrimination (Figure S2D−F).[37,38] The observed PC−NTC separation grows over time because miRNA−probe binding in the PC delays dimer formation relative to the NTC. Primer titration showed that 250 nM equimolar FP and RP primers produced the fastest amplification and greatest PC−NTC separation, outperforming both 100 nM and the TwistDx-recommended 480 nM (Figure S2G−H). Using equimolar primers prevents asymmetric amplification that would exhaust one primer prematurely. These optimized conditions minimize off-target interactions, delay dimer formation in the PC, and ensure a pronounced divergence of the amplification kinetics from the NTC as the reaction proceeds.

For severe SARS-CoV-2 infection in children, two additional target miRNAs are identified: miR-296 and miR-29. For each potential miRNA, a set of two ligation probes (P1 and P2) was designed for the ligation reaction (Figure 1B), and two primers were planned to amplify the ligation products for miR-296 and miR-29 (Tables S1−S3). We also validated the feasibility of the reaction platform for miR-296 and miR-29 at 100 pM target concentrations, respectively (Figure 1E,F). The results showed that our platform was able to detect miR-1273, miR-296, and miR-29 effectively. Figure S1B,C demonstrated the raw signal for miR-296 and miR-29. Based on the above discussion, we consider using ΔRFU instead of a direct RFU signal for the assay readout. The total detection procedures were simple and rapid, ∼42 min without thermal cycles, enabling miRNA detection of pediatric SARS-CoV-2 infection. Our current assay operates as a multiplex parallel system using nonspecific probes; however, transitioning to a true one-pot format with specifically designed probes could enhance sensitivity and reduce assay time. Nonetheless, this improvement may come at the expense of increased cost, highlighting the inherent trade-off between sensitivity and affordability in assay development.

Design and Validation of the Portable Analyzer. To translate this assay into a portable analytical tool, we designed and developed a compact, portable fluorescent analyzer and determined the resolution of miRNA with this device. The portable analyzer consists of 8 sample wells, including 11.5 cm in length, 7.5 cm in width, and 7 cm in height. This device is closely based on the current state-of-the-art multiplex target detection model developed by our group.[48−50] We have designed the device to support isothermal reactions and single-target detection using the cyan channel (500−520 nm) for single-wavelength measurement its eight detection channels, as shown in Figure 2A. The small size of the detection device allows patients to test samples for multiplexed analysis at POCT.[51,52] Our portable device connects to a smartphone via a user-friendly app that enables real-time monitoring of fluorescence curves and result interpretation. Central to this system is a custom-designed printed circuit board (PCB) that integrates thermal regulation, optical sensing, and data processing on a unified platform. A 7.4 V, 2200 mAh Li-ion battery powers the Raspberry Pi-based control unit, LEDs, and color sensors, while regulating the process to ensure precise temperature feedback and stability. These components are enclosed within a 3D-printed ABS casing for protection and structural support. The PCB layout is optimized to reduce noise interference between heating, pumping, and optical sensing lines, ensuring a stable power delivery and accurate signal acquisition. As shown in Figure 2B, we integrated a low-cost, compact, and highly sensitive AS7431 color sensor into the device, eliminating the need for conventional optical filters. Specifically, an intercalating dye, SYTO 9, is excited by a blue LED, and the color sensor captures the emission. To ensure consistent ligation-RPA conditions, a power resistor is mounted beneath a custom-fabricated aluminum plate, integrating an MC65F103A NTC 10 kΩ microthermistor for continuous temperature monitoring. Real-time fluorescence intensity is recorded, analyzed, and interpreted through a software algorithm on a smartphone, calibrating the results to eliminate baseline offset. The device is powered by a DC jack using a 9 V battery. Its filter-free optical design significantly reduces both the size and complexity. This miniaturized, user-friendly, and cost-effective device has promising potential for miRNA detection in primary medical facilities.

Analytical Sensitivity in the Portable Device. To evaluate the analytical sensitivity of the assay and resolving capabilities of the portable device, we tested the synthesized miRNA samples, which are miR-1273, 296, and 29 concentrations from 1 fM to 100 pM. For severe SARS-CoV-2 cases, the miRNA concentrations are downregulated and exist at approximately 1 fM,[41] so resolving 1fM is crucial for the portable analyzer. In Figure 2B−D, following the hybridization, annealing and ligation reaction, we measured the ΔRFU signals of miR-1273, miR-296, and miR-29 of the RPA reaction using the portable analyzer. We tested the concentrations of 100 pM, 10 pM, 1 pM, 100 fM, 10 fM, 8 fM, 5 fM, 2 fM, and 1 fM for all three miRNAs. Four reactions were run for each miRNA for the lower concentrations (10 fM, 8 fM, 5 fM, 2 fM, and 1 fM). We resolved the minimum 1 fM

https://doi.org/10.1021/acssensors.5c01275
ACS Sens. 2025, 10, 5150−5159

concentrations for each target. We partitioned the miRNAs into three samples and added them to three sample wells, including a negative control in the other sample well. Each tube in various sample wells contained specific probes and primers to ligase and amplify each corresponding miRNA. The sequences of primers are shown in Tables S1−S3. The results showed a noticeable reaction time difference between positive and negative samples for each miRNA over threshold lines (100.43 AU). The threshold was determined using the raw NTC data shown in Figure S3A−C and calculating from the $\mu + 3\sigma$, where μ and σ stand for the mean and standard deviation of the signal, respectively. It demonstrated that our principle of ligation-RPA can successfully pick up signals from various miRNAs from 1 fM to 100 pM for multiplexed miRNA detection. In Figure S4, the 1 fM signal is closer to the threshold line than the NTC. Below 1 fM, 500 and 800 aM did not produce signals above the threshold line.

To validate the quantitative capabilities of the portable device, we evaluated the linearity of the assay. As shown in Figure 2E−G, we calculated time as positive '(T_t)' values when the ΔRFU crosses the threshold line. miR-1273, miR-296, and miR-29 displayed R^2 values of 0.90, 0.85, and 0.97, respectively, and correlation coefficient r-values of 0.95, 0.92, and 0.98, respectively. The R^2 values indicate a strong proportion of variance in each measurement. Similarly, r values show a positive correlation of data. These results showed that the ligation-RPA assay was able to effectively detect various concentrations of miRNAs up to 1 fM. This suggests that our portable device is precise, consistent, and reliable for miRNA assay detection. These features make our device well-suited for the portable analysis of multiplex assays. Furthermore, we did not explore sensitivity below 1 fM, as this level meets clinical relevance and represents the practical resolution limit of our assay. To show the resolution capability of measuring each miRNA target using portable devices, we presented the t-test results with a bar plot. In Figure 2H−J, we found that we can differentiate 1 fM concentration with the t-test result with a p-value <0.05, which means the difference between the two groups is distinguishable at a 95% confidence interval (CI) level. However, the results look similar in two consecutive data points in a few cases. For instance, for miR-1273, 5 fM and 8 fM, and for miR-296, 1 fM and 2 fM showed similar kinds of ΔRFU and corresponding T_t, which were labeled 'ns' (not significant), showing no statistically significant difference. To clarify, we showed 1−10 fM results separately in Figure S3D−F. The result demonstrated that with the increased concentration of the miRNA sample, the T_t value decreased, which can be set as a positive reference for the clinical sample to evaluate unknown concentration. It also shows that both the device and the assay perform better and are usable for clinically relevant concentrations for severe-case miRNA.

Analytical Specificity in the Portable Device. To further validate the cross-reactivity of our assay, the specificity of the platform is essential for detecting specific miRNAs within abundant human saliva samples. We need to inspect the interferents of the signal of the miRNA assay against the other two types of miRNA targets, as inferred targets, to investigate the specificity for evaluating the detection capability. High concentrations of miRNAs (10 pM) were used in the miR-1273, miR-296, and miR-29 assays. As illustrated in Figure 3A, the first row displays results for the NTC sample, showing no amplification. In the second row, the specificity test for miR-

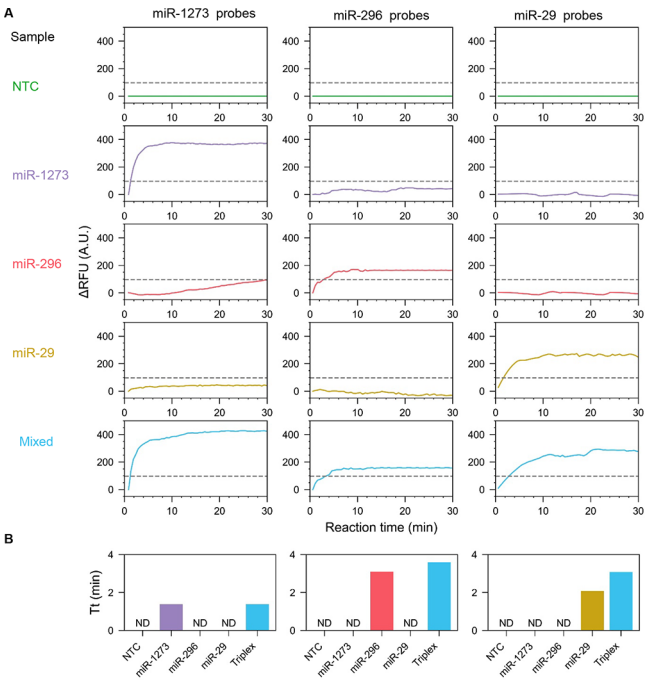

Figure 3. Specificity of the assay. (A) ΔRFU signals of NTC, miR-1273, miR-296, miR-29, and mixed miRNAs, represented with different colors. (B) Bar plot of T_t values for NTC, miR-1273, miR-296, miR-29, and mixed miRNAs. 'ND' indicates 'Not Detected', meaning the signals did not cross the threshold ($\mu + 3\sigma$ = 100.43 A.U.). The gray dashed line represents the threshold.

1273 demonstrates that amplification occurs only with miR-1273 probes (P1 and P2), while no amplification is observed with other probes such as miR-296 and miR-29 probes. Similarly, in the third and fourth rows, specific targets miR-296 and miR-29 only amplify when mixed with their respective probes. In the last row, a triplex sample containing miR-1273, miR-296, and miR-29 produces a signal for all probe types in the ligation-RPA assay, indicating that each target in the triplex sample is detected by its corresponding probe (for example, miR-1273 in the triplex mixture is detected by miR-1273 probes P1 and P2). However, slight variations in the initial and plateau phases of ΔRFU values, compared to those in Figure 2B−D, may stem from differences in experimental handling, such as timing of mixing, ice incubation conditions, or reagent variability, but these factors do not affect the overall assay specificity, as target miRNAs consistently yield distinct and selective amplification only with their corresponding probes.

To compare the specificity of each miRNA and the triplex miRNA assay, we present a bar plot of the T_t values for five cases: NTC, miR-1273, miR-296, miR-29, and triplex samples. In Figure 3B, the left panel shows that only the miR-1273 and triplex sample signals were detected, with T_t values of less than 2 min. Similarly, the middle panel indicates detection of miR-296 and triplex sample, while the right panel shows detection of miR-29 and the triplex sample. The reaction time of miR-1273 was approximately similar to that of the mixture of miRNAs. It indicated that the interfering miRNAs did not affect the miRNA-1273 detection. These results demonstrated that the miR-1273 assay has a high specificity, accurately recognizing the target miR-1273. Finally, we investigated the effects of miR-296 and miR-29 on miR-1273. The results exhibited 100% specificity of the assay. These results

https://doi.org/10.1021/acssensors.5c01275
ACS Sens. 2025, 10, 5150−5159

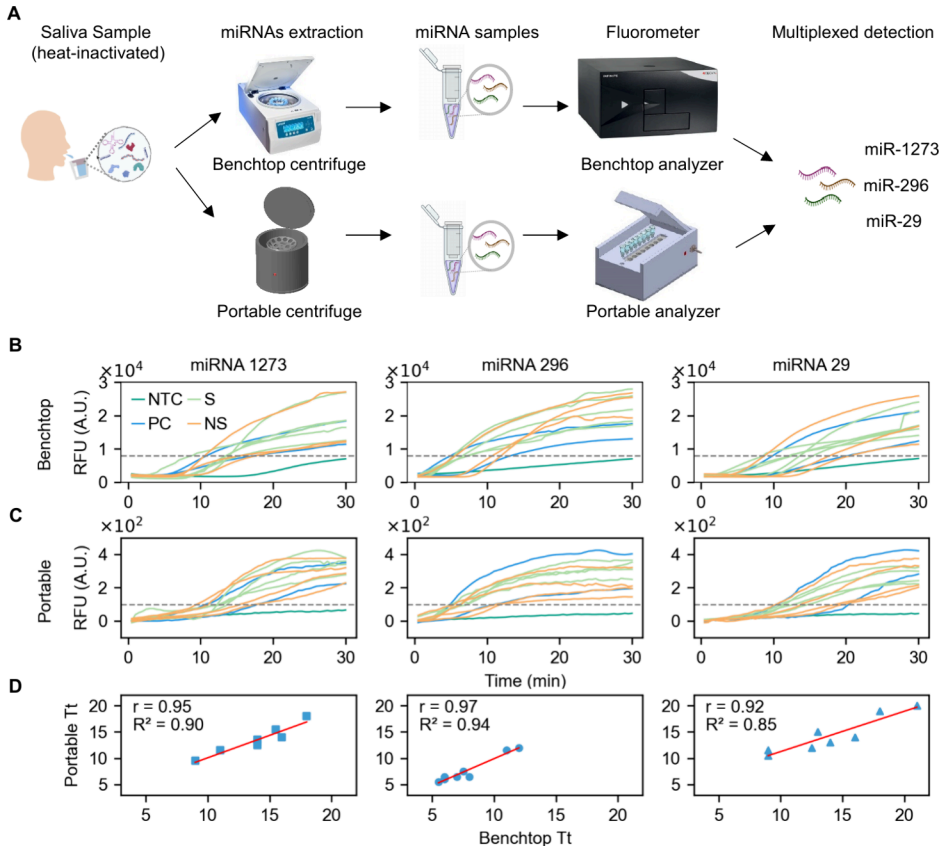

Figure 4. Validation of portable extraction and analyzer. (A) Schematic diagram of the workflow, illustrating the process from saliva collection to the readout of multiplex detection. Portable and benchtop extraction and analyzers are used in the intermediate steps. (B) RFU values from the benchtop analyzer for six nonsevere and two severe samples, with the threshold set at $\mu + 3\sigma$ = 7997 A.U. (C) RFU values from the portable analyzer for the same samples, with the threshold calculated as $\mu + 3\sigma$ = 100.43 A.U. (D) Comparison of T_t values between the portable and benchtop analyzers, including R^2 and r values for miR-1273, miR-296, and miR-29, respectively.

demonstrated that our platform successfully analyzes clinically complex miRNA samples.

Design and Validation of Portable miRNA Extraction. To evaluate the performance of our assay in detecting the viral presence in clinical and field scenarios, we conducted an extended sensitivity comparison against standard benchtop extraction methods. Using multiplexed miRNA detection on a portable extraction system, we tested eight clinical samples, including two severe and six nonsevere cases, with positive reference concentrations of 100 fM, 10 fM, and 1 fM. Saliva swabs were collected with DNA Genotek kits (proprietary nucleic acid solution). Our group developed an integrated platform with extraction reagents and portable centrifuge devices to purify miRNAs in saliva. This semi-automated platform allows users to easily extract miRNAs from saliva.[53,54] We employed the commercial miRNA extraction Kit to extract all of the miRNAs from saliva to obtain the practical content of target miRNAs. Figure 4A shows the workflow of multiplex detection of clinical samples. The process includes saliva collection, sample extraction using a portable or benchtop centrifuge, and multiplex detection using a portable or benchtop analyzer.

First, to compare the performance of our portable analyzer with that of the commercial Tcan analyzer, we analyzed the amplification curves generated for the miR-1273, miR-296, and miR-29 types on a benchtop centrifuge and analyzer. Figure 4B presents the ΔRFU signal for all eight clinical samples for three different miRNAs using benchtop devices. We simultaneously targeted 3 different miRNA samples with 3 PC: 100 fM, 10 fM, and 1 fM, and one NTC. The threshold was set to 7997 A.U. for this detection. From this threshold, we evaluated the T_t values for all samples. Furthermore, we need to verify the workability of portable centrifuge device since it is being used for miRNA samples for the first time. Each sample was divided into two equal aliquots of 300 μL; one was extracted using a benchtop centrifuge, and a portable centrifuge was used for the other. Figure S5 presents the total RNA concentrations of 6 nonsevere and 2 severe clinical samples using a NanoDrop, and the results are compared with those of the benchtop centrifuge. The portable centrifuge shows a strong linear fit with R^2 values of 0.93 and a strong positive correlation with an r value of 0.97. After successful extraction, we used our portable analyzer to acquire the RFU signal from the assay.

To demonstrate the quantification capabilities of the portable analyzer for eight clinical samples, we processed the miRNA extracted using the portable centrifuge to detect miR-1273, miR-296, and miR-29. Figure 4C presents the ΔRFU signal for all eight clinical samples for three different miRNAs using a portable extraction and analyzer. The threshold value was set at 100.43 A.U. Finally, to demonstrate the consistency between the benchtop and portable systems, we compared the T_t values presented in Figure 4D. The R^2 values for miR-1273, miR-296, and miR-29 were 0.90, 0.94, and 0.85, respectively, with corresponding r values of 0.95, 0.97, and 0.92. These results confirm the strong concordance between the two systems, highlighting the capability of portable device to

https://doi.org/10.1021/acssensors.5c01275
ACS Sens. 2025, 10, 5150−5159

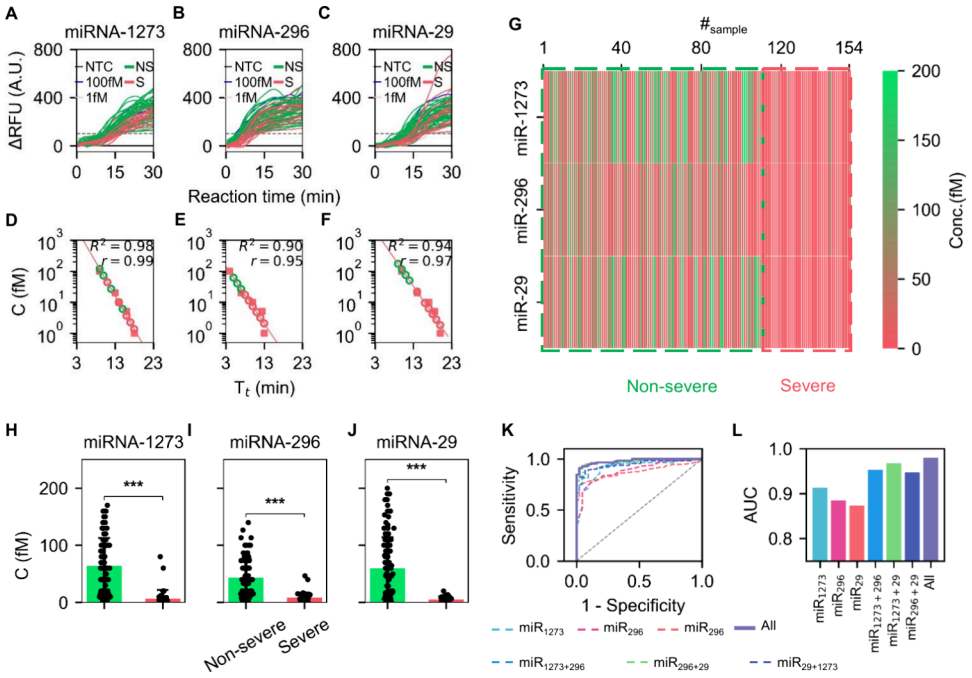

Figure 5. Testing of clinical raw salivary samples. (A−C) ΔRFU signals of miR-1273, miR-296, and miR-29 from 154 clinical samples, including 111 nonsevere and 43 severe cases. The gray dashed line represents the threshold (μ + 3σ = 100.43 A.U.). Green and red colors indicate nonseverity and severity, respectively. (D−F) Calibration plots determine unknown T_t values using known T_t values. (G) Heat map presenting the 154 clinical samples, with a red-to-green color gradient indicating low to high concentrations. (H−J) Bar plots comparing nonsevere and severe samples, where *** indicates statistical significance with a p-value <0.001. (K) The ROC-AUC plot shows that combined miRNA testing outperforms individual and dual combinations miRNA testing regarding AUC values. (L) Barplot to show the comparison of the single, dual, and combined miRNA testing results.

deliver results comparable to the benchtop system with high accuracy and reliability. Our results establish the applicability of the portable extraction system as an alternative to conventional laboratory methods. The portable analyzer demonstrated exceptional utility for accurately quantifying miRNAs. The high sensitivity, specificity, and consistency of multiplex assay in a portable format make it a valuable tool for real-time diagnostics of clinical SARS-CoV-2 miRNA samples, especially in areas where traditional laboratory infrastructure is unavailable.

Downregulation of miRNAs in Severe Clinical Samples. To investigate the profiling and prediction of unknown severe and nonsevere SARS-CoV-2 miRNA, we tested 154 clinical SARS-CoV-2 samples. The detection of miRNA in concentrations within the fM level requires high sensitivity and accuracy.[55] We tested 43 severe and 111 nonsevere clinical samples with internal PC samples of 100 fM, 20 fM, 10 fM, and 1 fM. Figure 5A−C shows the quantitative measurements of all 154 samples for miR-1273, miR-296, and miR-29. The results demonstrated that all miRNAs underwent successful ligation and RPA amplification, with each crossing the detection threshold. Next, to determine the concentrations of 154 unknown samples, we utilized PC for calibration. Using the T_t values obtained from PC samples with known concentrations of 100 fM, 20 fM, 10 fM, and 1 fM, we calibrated the concentrations of miRNA targets in the 154 unknown severe and nonsevere samples. Figure 5D−F presents the calibration results of miR-1273, miR-296, and miR-29, respectively. We measured the R^2 values for miR-1273, miR-296, and miR-29, which were 0.98, 0.90, and 0.94, respectively, with corresponding r values of 0.99, 0.95, and 0.97. The result indicates that the calibration method is highly accurate and reliable, demonstrating strong linearity and correlation.

To visualize the concentration profiles of miR-1273, miR-296, and miR-29, a heat map of 154 clinical samples is shown in Figure 5G. From the heat map, it is clear that miRNA concentrations in severe samples are much lower than in nonsevere samples. The severe samples are reddish, whereas the nonsevere samples are greenish. The severe miRNA concentrations are mostly less than 10 fM, whereas the nonsevere sample has many miRNA variations from 10 fM to 200 fM. Scaling our extraction data (1−200 fM detected in the 10 μL test aliquot) by the elution-to-saliva ratio (40 μL of elute of 350 μL of saliva) places the native clinical saliva concentration at ≈11 fM−2.3 pM, confirming that the heat-map values represent true physiological levels.[56−59] Notably, the saliva of children with severe illness exhibited significantly decreased miR-1273, miR-296, and miR-29 levels.[1] The miR-1273, miR-296, and miR-29 are significant early severe SARS-CoV-2 infection markers. The results show that miRNA levels in severe cases are less than in nonsevere cases, with most of miR-1273, miR-29, and miR-296 downregulated.

To differentiate severe and nonsevere samples, we plotted bar plots and conducted t-tests between them for each miRNA sample in Figure 5H−J. The p-values are 2.34 × 10^{-9}, 5.28 × 10^{-7}, and 5.54 × 10^{-8}, respectively. These results indicate strong evidence against the null hypothesis, confirming statistically significant differences among the groups for all three miRNAs. These results suggest that the observed effects are highly unlikely to be due to random chance. The mean concentrations for miR-1273, miR-296, and miR-29 are 66.32 fM , 38.72 fM , and 63.85 fM for nonsevere samples, while 6.82 fM , 7.47 fM , and 4.75 fM for severe samples, respectively. In

https://doi.org/10.1021/acssensors.5c01275
ACS Sens. 2025, 10, 5150−5159

children with severe SARS-CoV-2 infection, the levels of salivary miRNA are downgraded compared with those with milder infections, with most miRNAs showing reduced expression.

Finally, to assess the trade-off between the sensitivity and specificity of measurement, we evaluated whether detecting a single miRNA is sufficient or if combining two or three miRNAs improves assay performance. Figure 5K compares single, dual, and combined miRNA detections, assessing their receiver operating characteristic (ROC)-AUC plot values across varying thresholds. To evaluate the AUC for single miRNAs, we used the raw concentration values of each miRNA as input features, assigning binary labels (1 for nonsevere and 0 for severe) to the samples. We computed the ROC curve by plotting the true positive rate (sensitivity) against the false positive rate (1-specificity) across various thresholds. We calculated the AUC value to quantify the ability of each miRNA to differentiate between the two groups. Additionally, for the dual and combined evaluation of miRNAs, we trained a logistic regression model using the concentrations of miR-1273, miR-296, and miR-29 as input features and sample labels (1 for nonsevere, 0 for severe) as outputs. The model assigned weights to each miRNA based on its contribution to the classification and generated predicted probabilities (scores) for the nonsevere class. These scores were used to compute the ROC curve and the AUC, reflecting the dual and combined discriminatory performance of either two or three miRNAs in distinguishing severe from nonsevere samples. The combined-miRNA AUC of 0.98 outperforms the dual-miRNA AUCs (0.95, 0.96, and 0.94) and the individual miRNA AUCs (0.91, 0.88, and 0.87), highlighting the improved accuracy of multi-miRNA detection, shown in Figure 5L. These results indicate that multiplexing enhances specificity and sensitivity compared to single-miRNA testing, albeit at a higher cost, but it offers superior confidence in distinguishing severe miRNA-associated conditions. Differentiating between nonsevere and severe samples is crucial for accurately assessing the severity of the condition of children's infection with SARS-CoV-2, which can help in more effective treatment for disease detection in a POC setting.

CONCLUSIONS

This work presents an end-to-end portable platform that enables multiplex femtomolar-level detection of salivary miRNAs (miR-1273, miR-296, and miR-29) associated with severe SARS-CoV-2 infection in children. We have developed an isothermal ligation-RPA assay for multiplexed detection of miRNAs, using a portable analyzer with a total assay time of 42 min: 2 min for annealing, 10 min for ligation, and 30 min for RPA. We also developed an eight-channel hand-held analyzer with eight sample wells to detect and resolve the miRNA at fM concentrations and a portable extraction device, which is highly reliable and unlikely to introduce errors. Our assay exhibited 100% specificity for target miRNAs, even in the presence of interfering targets. Finally, we tested 154 pediatric saliva samples (111 nonsevere and 43 severe) with internal controls, revealing that the combined detection of each miRNA down-regulated in severe cases yields an AUC = 0.98. In future work, we will eliminate remaining manual liquid-handling steps by lyophilizing reagents, specific probe design, enabling true one-pot multiplexing, and integrating lysis, hybridization, ligation, and amplification into a single "sample-to-answer" cartridge, advancing toward a fully automated, low-cost, and field-ready miRNA diagnostic for point-of-care use. This integration would simplify the workflow, making our portable analyzer a powerful tool for the early detection of SARS-CoV-2 miRNAs in children, particularly in POC settings.

MATERIALS AND METHODS

Materials and methods are described in the Supporting Information.

ASSOCIATED CONTENT

Data Availability Statement

Data from the study are available from the corresponding author upon reasonable request.

Supporting Information

The Supporting Information is available free of charge at https://pubs.acs.org/doi/10.1021/acssensors.5c01275.

Raw RFU traces for positive-control (PC) and no-template control (NTC) samples of miR-1273, miR-296, and miR-29; data on probe- and primer-concentration optimization for the miRNA-mediated ligation−RPA assay; validation results for the portable extraction device; supplementary tables listing primer sequences, reaction recipes, and cost breakdowns for both the reactions and the portable system (PDF)

End-to-end process of miRNA sample extraction and ligation-RPA detection (MP4)

AUTHOR INFORMATION

Corresponding Author

Weihua Guan − *Department of Intelligent Systems Engineering, Luddy School of Informatics, Computing, and Engineering, Indiana University, Bloomington, Indiana 47408, United States;* orcid.org/0000-0002-8435-9672; Email: guanw@iu.edu

Authors

Md. Ahasan Ahamed − *Department of Intelligent Systems Engineering, Luddy School of Informatics, Computing, and Engineering, Indiana University, Bloomington, Indiana 47408, United States; Department of Electrical Engineering, Pennsylvania State University, University Park, Pennsylvania 16802, United States;* orcid.org/0009-0006-9962-2994

Zhikun Zhang − *Department of Electrical Engineering, Pennsylvania State University, University Park, Pennsylvania 16802, United States*

Aneesh Kshirsagar − *Department of Electrical Engineering, Pennsylvania State University, University Park, Pennsylvania 16802, United States;* orcid.org/0000-0003-2288-5439

Anthony J. Politza − *Department of Biomedical Engineering, Pennsylvania State University, University Park, Pennsylvania 16802, United States;* orcid.org/0009-0005-8670-2357

Usha Sethuraman − *Division of Emergency Medicine, Department of Pediatrics, Children's Hospital of Michigan/Central Michigan University, Detroit, Michigan 48201, United States*

Srinivasan Suresh − *Divisions of Health Informatics and Emergency Medicine, Department of Pediatrics, University of Pittsburgh School of Medicine and UPMC Children's Hospital of Pittsburgh, Pittsburgh, Pennsylvania 15224, United States*

Steven Hicks − *Department of Pediatrics, Division of Academic General Pediatrics, Penn State Neuroscience*

https://doi.org/10.1021/acssensors.5c01275
ACS Sens. 2025, 10, 5150−5159

Institute, Pennsylvania State University, Hershey, Pennsylvania 17033, United States

Feng Guo − *Department of Intelligent Systems Engineering, Luddy School of Informatics, Computing, and Engineering, Indiana University, Bloomington, Indiana 47408, United States;* orcid.org/0000-0001-9103-3235

Complete contact information is available at: https://pubs.acs.org/10.1021/acssensors.5c01275

Author Contributions

Z.Z. and M.A.A. designed and validated the assay. M.A.A. performed clinical sample testing and validation. M.A.A., Z.Z., and F.G. conducted data analysis. A.K. developed the portable analytical device. A.J.P. developed the portable sample extraction device. S.H., U.S., and S.S. collected clinical samples and provided clinical insight into the significance of miRNA related to COVID-19 severity. W.G. developed the concept and supervised the overall experiment design. M.A.A., Z.Z., and W.G. cowrote the manuscript with input from others. M.A.A. and Z.Z. contributed equally to this work.

Funding

This work was partially supported by the Eunice Kennedy Shriver National Institute of Child Health & Human Development of the National Institutes of Health through the RADx program (1R61HD105610), the National Institutes of Health (R33HD105610, R33AI147419), and the National Science Foundation (2319913). Any opinions, findings, conclusions, or recommendations expressed in this work are those of the authors and do not necessarily reflect the views of the National Science Foundation and National Institutes of Health.

Notes

A preprint of this article was posted on medRxiv on March 11, 2025 (doi: 10.1101/2025.03.10.25323665).

The authors declare the following competing financial interest(s): A provisional patent has been filed related to the technology described herein.

REFERENCES

(1) Hicks, S. D.; Zhu, D.; Sullivan, R.; Kannikeswaran, N.; Meert, K.; Chen, W.; Suresh, S.; Sethuraman, U. Saliva microRNA Profile in Children with and without Severe SARS-CoV-2 Infection. *Int. J. Mol. Sci.* **2023**, *24* (9), 8175.

(2) Huang, C.; Wang, Y.; Li, X.; Ren, L.; Zhao, J.; Hu, Y.; Zhang, L.; Fan, G.; Xu, J.; Gu, X.; Cheng, Z.; Yu, T.; Xia, J.; Wei, Y.; Wu, W.; Xie, X.; Yin, W.; Li, H.; Liu, M.; Xiao, Y.; Gao, H.; Guo, L.; Xie, J.; Wang, G.; Jiang, R.; Gao, Z.; Jin, Q.; Wang, J.; Cao, B. Clinical Features of Patients Infected with 2019 Novel Coronavirus in Wuhan. *China. The Lancet* **2020**, *395* (10223), 497−506.

(3) Hu, B.; Guo, H.; Zhou, P.; Shi, Z.-L. Characteristics of SARS-CoV-2 and COVID-19. *Nat. Rev. Microbiol.* **2021**, *19* (3), 141−154.

(4) CDC *Child mortality and COVID-19*; United Nations Children's Fund. https://data.unicef.org/topic/child-survival/covid-19/ (accessed Feb 12, 2025).

(5) Murray, S. M.; Ansari, A. M.; Frater, J.; Klenerman, P.; Dunachie, S.; Barnes, E.; Ogbe, A. The Impact of Pre-Existing Cross-Reactive Immunity on SARS-CoV-2 Infection and Vaccine Responses. *Nat. Rev. Immunol.* **2023**, *23* (5), 304−316.

(6) Huang, H.; Fan, C.; Li, M.; Nie, H.-L.; Wang, F.-B.; Wang, H.; Wang, R.; Xia, J.; Zheng, X.; Zuo, X.; Huang, J. COVID-19: A Call for Physical Scientists and Engineers. *ACS Nano* **2020**, *14* (4), 3747−3754.

(7) Welch, N. L.; Zhu, M.; Hua, C.; Weller, J.; Mirhashemi, M. E.; Nguyen, T. G.; Mantena, S.; Bauer, M. R.; Shaw, B. M.; Ackerman, C. M.; Thakku, S. G.; Tse, M. W.; Kehe, J.; Uwera, M.-M.; Eversley, J. S.; Bielwaski, D. A.; McGrath, G.; Braidt, J.; Johnson, J.; Cerrato, F.; Moreno, G. K.; Krasilnikova, L. A.; Petros, B. A.; Gionet, G. L.; King, E.; Huard, R. C.; Jalbert, S. K.; Cleary, M. L.; Fitzgerald, N. A.; Gabriel, S. B.; Gallagher, G. R.; Smole, S. C.; Madoff, L. C.; Brown, C. M.; Keller, M. W.; Wilson, M. M.; Kirby, M. K.; Barnes, J. R.; Park, D. J.; Siddle, K. J.; Happi, C. T.; Hung, D. T.; Springer, M.; MacInnis, B. L.; Lemieux, J. E.; Rosenberg, E.; Branda, J. A.; Blainey, P. C.; Sabeti, P. C.; Myhrvold, C. Multiplexed CRISPR-Based Microfluidic Platform for Clinical Testing of Respiratory Viruses and Identification of SARS-CoV-2 Variants. *Nat. Med.* **2022**, *28* (5), 1083−1094.

(8) Najjar, D.; Rainbow, J.; Sharma Timilsina, S.; Jolly, P.; De Puig, H.; Yafia, M.; Durr, N.; Sallum, H.; Alter, G.; Li, J. Z.; Yu, X. G.; Walt, D. R.; Paradiso, J. A.; Estrela, P.; Collins, J. J.; Ingber, D. E. A Lab-on-a-Chip for the Concurrent Electrochemical Detection of SARS-CoV-2 RNA and Anti-SARS-CoV-2 Antibodies in Saliva and Plasma. *Nat. Biomed. Eng.* **2022**, *6* (8), 968−978.

(9) Ahamed, M. A.; Politza, A. J.; Liu, T.; Khalid, M. A. U.; Zhang, H.; Guan, W. CRISPR-Based Strategies for Sample-to-Answer Monkeypox Detection: Current Status and Emerging Opportunities. *Nanotechnology* **2025**, *36* (4), No. 042001.

(10) Zhang, Z.; Liu, T.; Dong, M.; Ahamed, Md. A.; Guan, W. Sample-to-Answer Salivary miRNA Testing: New Frontiers in Point-of-Care Diagnostic Technologies. *WIREs Nanomedicine Nanobiotechnology* **2024**, *16* (3), No. e1969.

(11) Tribolet, L.; Kerr, E.; Cowled, C.; Bean, A. G. D.; Stewart, C. R.; Dearnley, M.; Farr, R. J. MicroRNA Biomarkers for Infectious Diseases: From Basic Research to Biosensing. *Front. Microbiol.* **2020**, *11*, 1197.

(12) Ojha, R.; Nandani, R.; Pandey, R. K.; Mishra, A.; Prajapati, V. K. Emerging Role of Circulating microRNA in the Diagnosis of Human Infectious Diseases. *J. Cell. Physiol.* **2019**, *234* (2), 1030−1043.

(13) Garcia-Martin, R.; Wang, G.; Brandão, B. B.; Zanotto, T. M.; Shah, S.; Kumar Patel, S.; Schilling, B.; Kahn, C. R. MicroRNA Sequence Codes for Small Extracellular Vesicle Release and Cellular Retention. *Nature* **2022**, *601* (7893), 446−451.

(14) Zhang, Z.; Ahamed, M. A.; Yang, D. Biological Properties and DNA Nanomaterial Biosensors of Exosomal miRNAs in Disease Diagnosis. *Sens. Diagn.* **2025**, *4*, 273−292.

(15) Abu-Izneid, T.; AlHajri, N.; Ibrahim, A. M.; Javed, Md. N.; Salem, K. M.; Pottoo, F. H.; Kamal, M. A. Micro-RNAs in the Regulation of Immune Response against SARS CoV-2 and Other Viral Infections. *J. Adv. Res.* **2021**, *30*, 133−145.

(16) Bartoszewski, R.; Dabrowski, M.; Jakiela, B.; Matalon, S.; Harrod, K. S.; Sanak, M.; Collawn, J. F. SARS-CoV-2 May Regulate Cellular Responses through Depletion of Specific Host miRNAs. *Am. J. Physiol.-Lung Cell. Mol. Physiol.* **2020**, *319* (3), L444−L455.

(17) Kobayashi, H.; Singer, R. H. Single-Molecule Imaging of microRNA-Mediated Gene Silencing in Cells. *Nat. Commun.* **2022**, *13* (1), 1435.

(18) Bentahir, M.; Ambroise, J.; Delcorps, C.; Pilo, P.; Gala, J. L. Sensitive and Specific Recombinase Polymerase Amplification Assays for Fast Screening, Detection, and Identification of Bacillus Anthracis in a Field Setting. *Appl. Environ. Microbiol.* **2018**, *84* (11), No. e00506-18.

(19) Husale, S.; Persson, H. H. J.; Sahin, O. DNA Nanomechanics Allows Direct Digital Detection of Complementary DNA and microRNA Targets. *Nature* **2009**, *462* (7276), 1075−1078.

(20) Valoczi, A. Sensitive and Specific Detection of microRNAs by Northern Blot Analysis Using LNA-Modified Oligonucleotide Probes. *Nucleic Acids Res.* **2004**, *32* (22), e175−e175.

(21) Chen, J.; Lozach, J.; Garcia, E. W.; Barnes, B.; Luo, S.; Mikoulitch, I.; Zhou, L.; Schroth, G.; Fan, J.-B. Highly Sensitive and Specific microRNA Expression Profiling Using BeadArray Technology. *Nucleic Acids Res.* **2008**, *36* (14), e87−e87.

(22) Pan, X.; Murashov, A. K.; Stellwag, E. J.; Zhang, B. Monitoring MicroRNA Expression During Embryonic Stem-Cell Differentiation Using Quantitative Real-Time PCR (qRT-PCR). In *RNAi and*

microRNA-Mediated Gene Regulation in Stem Cells; Zhang, B., Stellwag, E. J., Eds.; Methods in Molecular Biology; Humana Press: Totowa, NJ, 2010; Vol. *650*, pp 213−224.
(23) Trevino, V.; Falciani, F.; Barrera-Saldaña, H. A. DNA Microarrays: A Powerful Genomic Tool for Biomedical and Clinical Research. *Mol. Med.* **2007**, *13* (9−10), 527−541.
(24) Villaseñor-Altamirano, A. B.; Balderas-Martínez, Y. I.; Medina-Rivera, A. Review of Gene Expression Using Microarray and RNA-Seq. In *Rigor and Reproducibility in Genetics and Genomics*; Elsevier, 2024; pp 159−187.
(25) Gonzalo, R.; Sánchez, A. Introduction to Microarrays Technology and Data Analysis. In *Comprehensive Analytical Chemistry*; Elsevier, 2018; Vol. *82*, pp 37−69.
(26) Khalid, M. A. U.; Ahamed, Md. A.; Dong, M.; Kshirsagar, A.; Guan, W. Hydrogel Interfaced Glass Nanopore for High-Resolution Sizing of Short DNA Fragments. *Biosens. Bioelectron.* **2025**, *268*, No. 116895.
(27) Lan, L.; Huang, J.; Liu, M.; Yin, Y.; Wei, C.; Cai, Q.; Meng, X. Polymerization and Isomerization Cyclic Amplification for Nucleic Acid Detection with Attomolar Sensitivity. *Chem. Sci.* **2021**, *12* (12), 4509−4518.
(28) Feng, S.; Chen, H.; Hu, Z.; Wu, T.; Liu, Z. Ultrasensitive Detection of miRNA via CRISPR/Cas12a Coupled with Strand Displacement Amplification Reaction. *ACS Appl. Mater. Interfaces* **2023**, *15* (24), 28933−28940.
(29) Li, D.; Zhang, T.; Yang, F.; Yuan, R.; Xiang, Y. Efficient and Exponential Rolling Circle Amplification Molecular Network Leads to Ultrasensitive and Label-Free Detection of MicroRNA. *Anal. Chem.* **2020**, *92* (2), 2074−2079.
(30) Dong, M.; Kshirsagar, A.; Politza, A. J.; Khalid, M. A. U.; Ahamed, M. A.; Guan, W. Addressing Buffer, Size, and Clogging Challenges in LAMP-Coupled Solid-State Nanopores for Point-of-Care Testing. *Anal. Chem.* **2025**, *97*, 7879−7887.
(31) Koo, K. M.; Wee, E. J. H.; Trau, M. High-Speed Biosensing Strategy for Non-Invasive Profiling of Multiple Cancer Fusion Genes in Urine. *Biosens. Bioelectron.* **2017**, *89*, 715−720.
(32) Li, J.; Macdonald, J. Advances in Isothermal Amplification: Novel Strategies Inspired by Biological Processes. *Biosens. Bioelectron.* **2015**, *64*, 196−211.
(33) Ahamed, Md. A.; Khalid, M. A. U.; Dong, M.; Politza, A. J.; Zhang, Z.; Kshirsagar, A.; Liu, T.; Guan, W. Sensitive and Specific CRISPR-Cas12a Assisted Nanopore with RPA for Monkeypox Detection. *Biosens. Bioelectron.* **2024**, *246*, No. 115866.
(34) Ahamed, Md. A.; Guan, W. CRISPR-Assisted Solid-State Nanopore Sensor for Rapid and Sensitive Point-of-Care Amendable of Monkeypox Virus Detection via RPA Amplification. *Biophys. J.* **2024**, *123* (3), 145a.
(35) Oliveira, B. B.; Veigas, B.; Baptista, P. V. Isothermal Amplification of Nucleic Acids: The Race for the Next "Gold Standard.". *Front. Sens.* **2021**, *2*, No. 752600.
(36) Preena, P. G.; Kumar, T. V. A.; Johny, T. K.; Dharmaratnam, A.; Swaminathan, T. R. Quick Hassle-Free Detection of Cyprinid Herpesvirus 2 (CyHV-2) in Goldfish Using Recombinase Polymerase Amplification-Lateral Flow Dipstick (RPA-LFD) Assay. *Aquac. Int.* **2022**, *30* (3), 1211−1220.
(37) Wee, E. J. H.; Trau, M. Simple Isothermal Strategy for Multiplexed, Rapid, Sensitive, and Accurate miRNA Detection. *ACS Sens.* **2016**, *1* (6), 670−675.
(38) Wang, P.; Ma, C.; Zhang, X.; Chen, L.; Yi, L.; Liu, X.; Lu, Q.; Cao, Y.; Gao, S. A Ligation/Recombinase Polymerase Amplification Assay for Rapid Detection of SARS-CoV−2. *Front. Cell. Infect. Microbiol.* **2021**, *11*, No. 680728.
(39) Yao, X.-C.; Wu, J.-J.; Yuan, S.-T.; Yuan, F.-L. Recent Insights and Perspectives into the Role of the miRNA-29 Family in Innate Immunity (Review). *Int. J. Mol. Med.* **2025**, *55* (3), 53.
(40) Yan, H.; Wen, Y.; Tian, Z.; Hart, N.; Han, S.; Hughes, S. J.; Zeng, Y. A One-Pot Isothermal Cas12-Based Assay for the Sensitive Detection of microRNAs. *Nat. Biomed. Eng.* **2023**, *7* (12), 1583−1601.
(41) Kumar, N.; Shetti, N. P.; Jagannath, S.; Aminabhavi, T. M. Electrochemical Sensors for the Detection of SARS-CoV-2 Virus. *Chem. Eng. J.* **2022**, *430*, No. 132966.
(42) Bhagavan, N. V.; Ha, C.-E. Structure and Properties of DNA. In *Essentials of Medical Biochemistry*; Elsevier, 2015; pp 381−400.
(43) Ivanov, A. V.; Safenkova, I. V.; Zherdev, A. V.; Dzantiev, B. B. Multiplex Assay of Viruses Integrating Recombinase Polymerase Amplification, Barcode—Anti-Barcode Pairs, Blocking Anti-Primers, and Lateral Flow Assay. *Anal. Chem.* **2021**, *93* (40), 13641−13650.
(44) Meagher, R. J.; Priye, A.; Light, Y. K.; Huang, C.; Wang, E. Impact of Primer Dimers and Self-Amplifying Hairpins on Reverse Transcription Loop-Mediated Isothermal Amplification Detection of Viral RNA. *Analyst* **2018**, *143* (8), 1924−1933.
(45) Sharma, N.; Hoshika, S.; Hutter, D.; Bradley, K. M.; Benner, S. A. Recombinase-Based Isothermal Amplification of Nucleic Acids with Self-Avoiding Molecular Recognition Systems (SAMRS). *ChemBioChem.* **2014**, *15* (15), 2268−2274.
(46) Piepenburg, O.; Williams, C. H.; Stemple, D. L.; Armes, N. A. DNA Detection Using Recombination Proteins. *PLoS Biol.* **2006**, *4* (7), No. e204.
(47) Nolan, T.; Hands, R. E.; Bustin, S. A. Quantification of mRNA Using Real-Time RT-PCR. *Nat. Protoc.* **2006**, *1* (3), 1559−1582.
(48) Liu, T.; Politza, A. J.; Kshirsagar, A.; Zhu, Y.; Guan, W. Compact Point-of-Care Device for Self-Administered HIV Viral Load Tests from Whole Blood. *ACS Sens.* **2023**, *8*, 4716−4727.
(49) Liu, T.; Politza, A. J.; Ahamed, Md. A.; Kshirsagar, A.; Zhu, Y.; Guan, W. Compact Multiplex PCR Device for HIV-1 and HIV-2 Viral Load Determination from Finger-Prick Whole Blood in Resource-Limited Settings. *Biosens. Bioelectron.* **2025**, *271*, No. 116997.
(50) Kshirsagar, A.; Politza, A. J.; Guan, W. Deep Learning Enabled Universal Multiplexed Fluorescence Detection for Point-of-Care Applications. *ACS Sens.* **2024**, *9*, 4017.
(51) Luppa, P. B.; Müller, C.; Schlichtiger, A.; Schlebusch, H. Point-of-Care Testing (POCT): Current Techniques and Future Perspectives. *TrAC Trends Anal. Chem.* **2011**, *30* (6), 887−898.
(52) Song, Q.; Sun, X.; Dai, Z.; Gao, Y.; Gong, X.; Zhou, B.; Wu, J.; Wen, W. Point-of-Care Testing Detection Methods for COVID-19. *Lab. Chip* **2021**, *21* (9), 1634−1660.
(53) Politza, A. J.; Liu, T.; Kshirsagar, A.; Dong, M.; Ahamed, M. A.; Guan, W. *A Portable Centrifuge for Universal Nucleic Acid Extraction at the Point-of-Care*, Rochester, NY, April 3, 2024. https://doi.org/10.2139/ssrn.4781228.
(54) Politza, A. J.; Liu, T.; Kshirsagar, A.; Dong, M.; Ahasan Ahamed, Md.; Guan, W. *A Portable Device for Lab-Free, Versatile Nucleic Acid Extraction - Protocol*, October 14, 2024. https://doi.org/10.17504/protocols.io.kxygxyj4wl8j/v1.
(55) Jet, T.; Gines, G.; Rondelez, Y.; Taly, V. Advances in Multiplexed Techniques for the Detection and Quantification of microRNAs. *Chem. Soc. Rev.* **2021**, *50* (6), 4141−4161.
(56) Rapado-González, Ó.; Majem, B.; Álvarez-Castro, A.; Díaz-Peña, R.; Abalo, A.; Suárez-Cabrera, L.; Gil-Moreno, A.; Santamaría, A.; López-López, R.; Muinelo-Romay, L.; Suarez-Cunqueiro, M. M. A Novel Saliva-Based miRNA Signature for Colorectal Cancer Diagnosis. *J. Clin. Med.* **2019**, *8* (12), 2029.
(57) Patel, R. S.; Jakymiw, A.; Yao, B.; Pauley, B. A.; Carcamo, W. C.; Katz, J.; Cheng, J. Q.; Chan, E. K. L. High Resolution of microRNA Signatures in Human Whole Saliva. *Arch. Oral Biol.* **2011**, *56* (12), 1506−1513.
(58) Wu, Y.; Pei, J.; Li, Y.; Wang, G.; Li, L.; Liu, J.; Tian, G. High-Sensitive and Rapid Electrochemical Detection of miRNA-31 in Saliva Using Cas12a-Based 3D Nano-Harvester with Improved Trans-Cleavage Efficiency. *Talanta* **2024**, *266*, No. 125066.
(59) Li, J.; Zhang, W.; Chang, R.; Lan, Y.; Qiu, D.; Wang, K.; Huang, J.; Xu, Q. A Magnetic Separation-Assisted Auto-Cyclic Primer Extension for OSCC-Associated Salivary miRNA Detection. *Biosens. Bioelectron.* **2025**, *269*, No. 116936.

https://doi.org/10.1021/acssensors.5c01275
ACS Sens. 2025, 10, 5150−5159